Occurrence and Inhibition of Large Yawing Moments during High-Incidence Flight of Slender Missile Configurations

W. H. CLARK* AND J. R. PEOPLES†
Naval Weapons Center, China Lake, Calif.
AND
M. M. BRIGGS‡
McDonnell Douglas Astronautics Company, Huntington Beach, Calif.

This paper deals with the occurrence of asymmetric wake configurations, and associated side forces and yawing moments, during high-incidnce flight of slender, axisymmetric missile configurations. The relevant phenomena are characterized experimentally, and the root causes of wake asymmetries and means of inhibiting their occurrence are explored. It is concluded that certain flowfield disturbance devices may be effective in significantly reducing the maximum values of yawing moments induced by asymmetric disposition of wake vortices.

Nomenclature

A = reference area (usually $\pi d^2/4$)
α or α' = total angle of attack
$C_{d\infty}$ = drag coefficient of an infinite circular cylinder at given Mach number and Reynolds number
C_N' = normal force coefficient = (normal force in α' plane)/q_0A
C_n' = yawing moment coefficient = Moment acting $\perp$ to pitch plane, in plane of missile centerline)/q_0A
C_y' = side force coefficient = (Side force ($\perp$ to α' plane)/q_0A
d = reference diameter
η = finite cylinder correction factor
f = cross force per unit length
g' = quantity defined in Fig. 5 (vortex spacing)
Γ_1, Γ_2 = strengths of right and left vortices, respectively
l = configuration length
M = Mach number
$\phi_{(N, M)}$ = bank angle (of model nose or model body, respectively)
q_0 = freestream dynamic pressure
R = Local radius
R_{10}, R_{20} = initial radial positions of right and left vortices, respectively
R_{ed} = Reynolds number based on the missile principle diameter, d
S = Strouhal number
ds/dx = rate of change of body cross-sectional area with longitudinal distance along the body
θ_{10}, θ_{20} = angular position of right and left vortices, respectively
X = distance from vertex

Introduction

IN recent years, the introduction of high-performance missiles that maneuver at angles of attack as high as 180° has prompted a renewed interest in the basic aerodynamics of slender bodies of revolution. This classical problem has received considerable attention throughout the history of aeronautics because of the frequent use of relatively slender bodies in such applications as ballistic shells, rockets, dirigibles, and missiles. Since these early devices generally flew along more-or-less straight trajectories at low angles of attack, their aerodynamic performance was predictable through the use of potential flow analyses. For instance, the now-classical work of Munk,[1] which was based on the inviscid, incompressible flow about a circular cylinder, was used to predict the lift force due to cross flow about a dirigible by the following expression:

$$f = q_0\, ds/dx \sin 2\alpha \qquad (1)$$

This same expression is derived by Allen and Perkins.[2]

Later, Tsien[3] showed that the same expression is applicable to the prediction of lifting forces on slender bodies at low angles of attack for moderate supersonic speeds. The agreement between these theories demonstrates that even for high-speed flows, if the Mach number is not "too high" and if the angle of attack is low, then the cross flow Mach number will be low enough to fall within the incompressible flow regime.

It was recognised by these early investigators that a potential flow analysis was restricted to near-zero angles of attack and that at higher angles, the presence of viscosity would drastically alter the flow characteristics. The manner in which viscosity can effect the flow is illustrated in Fig. 1. Here the cross flow boundary layer separates due to the adverse pressure gradient on the lee side of the body, and the boundary-layer fluid "rolls up" into two cores of concentrated vorticity. These vortex cores can extend along almost the entire length of the body. The low pressures produced on the lee side greatly increase the lift (and drag) above those values predicted by the linear potential theories.

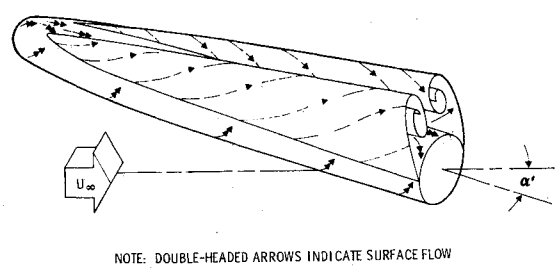

Fig. 1 Stable symmetric vortex separation (primary vortex pair only).

Presented as Paper 72-968 at the AIAA 2nd Atmospheric Flight Mechanics Conference, Palo Alto, Calif., September 11–13, 1972; submitted November 6, 1972; revision received April 11, 1973. The work reported here was performed for the U.S. Naval Weapons Center, China Lake, Calif. under Contracts N00123-69-C-0146-03 and N00123-71-C-0285. The authors gratefully acknowledge the assistance of W. Anderson, of the Advance Aero/Thermodynamics Department, McDonnell Douglas Astronautics Company, in performing the computer programming and other operations necessary to calculate vortex trajectories and resulting effects upon missile aerodynamics, using the methods described in Refs. 12 and 20.

Index category: Rocket Vehicle Aerodynamics.

* Aerospace Engineer, Preliminary Design Branch, Code 30102, Systems Development Department.

† Branch Head, Preliminary Design Branch, Code 30102, Systems Development Department.

‡ Senior Engineer, Advance Air-To-Air Missiles.

At this time there are no complete analytical techniques for quantitatively describing this phenomenon. There are, however, a number of semiempirical techniques that have been used with some success in accounting for these nonlinear viscous effects.

Allen and Perkins[2] accounted for the viscous cross flow in the following manner. They observed that for bodies at high angles of attack, the potential flow solutions resulted in surface pressure distribution "errors" similar to the lee-side pressure distribution of a two-dimensional cylinder, except for regions near the nose, where the axial flow still influences the local pressures. Hence, it would not be unreasonable to expect that the normal force at each axial station would be the same as that measured on a two-dimensional cylinder. They also assumed that the forces due to the viscous cross flow were directly additive to those from a potential flow analysis. The normal force per unit length becomes

$$f = q_0\, ds/dx \sin 2\alpha + 2RC_{d_\infty} q_0 \sin^2\alpha \qquad (2)$$

In practice, the potential contribution to this equation should be replaced by the Van Dyke[4] second-order theory for supersonic flows, and the drag coefficient should be corrected for the finite missile length. This same technique was expanded upon by Perkins and Jorgensen[5] to account empirically for the variation of the viscous cross force (C_{d_∞}) with axial position along the body.

Allen and Perkins[2] used the steady-state value for the drag coefficient, although they recognized that the attached body vortices on missile bodies were more analogous to the vortex patterns observed on two-dimensional cylinders in a transient, impulsively started flow. In the impulsively started flow ($M \ll 1$), the intial flowfield is essentially irrotational; but soon after starting, the boundary layer separates at the rear stagnation point, and two separation points propagate symmetrically away from this point. Eventually, at some angular distance from the rearward point, two regions of vorticity break away from the boundary layer, "rolling up" into two symmetrical vortex cores that propagate away from the body. Eventually, these vortex cores become asymmetrical and alternately discharge from the body, producing the familiar von Kármán vortex street or a turbulent wake for Reynolds numbers in excess of about 10^5 (aperiodic shedding). (This phenomenon is illustrated in Ref. 6). The flowfield about slender bodies of revolution is analogous to this transient flow because at various axial stations along the body the vortex formation resembles the vortex pair in the impulsive flow. Increasing distance from the nose of the three-dimensional flow corresponds to increasing time in the impulse flow.

Kelly[7] used this analogy by replacing the steady-state drag coefficient with a transient drag coefficient that he obtained from data by Schwabe.[8] That is, the viscous normal force contribution ($\Delta C_N'$) is given by

$$\Delta C_N' = \frac{2\eta \sin^2\alpha'}{A} \int_0^t RC_{D_\infty}(X)\, dX \qquad (3)$$

The function $C_{D_\infty}(X)$ is obtained in the following way. Schwabe presented the drag coefficient C_{D_∞} as a function of the dimensionless time Vt/R, as shown in Fig. 2. By replacing V with the normal velocity component $V_\infty \sin\alpha'$, and time t with $X/V_\infty \cos\alpha'$, the parameter Vt/R is replaced by $X/R \tan\alpha'$, which relates the cross flow drag to the axial station X.

Both Kelly's and Allen's[2] techniques for predicting normal forces have been used with some success at high angles of attack. Neither method, however, is accurate in predicting centers of pressure. The experiments of Perkins and Jorgensen[5] showed that the actual measured axial distribution of normal force on a tangent-ogive cylinder differed significantly from the theoretical values. In Fig. 2, the transient drag coefficient measured by Schwabe is compared with similar measurements taken by Sarpkaya.[9] Sarpkaya's data show that

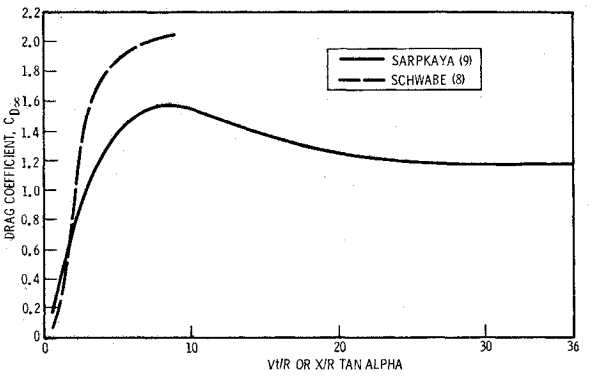

Fig. 2 Drag coefficient of impulsively started infinite cylinder v nondimensional time from start of motion.

C_{D_∞} asymptotically approaches the steady-state laminar value of $C_{D_\infty} = 1.2$ after a slight overshoot. In view of the differences between the two curves, and considering that Schwabe's data were taken at very low Reynolds numbers (560), it appears that the quantitative agreement between experiment and Kelly's theory may be somewhat fortuitous.

More recently, several techniques that consider the actual vortex structure have been developed.[10-12] In these theories, the viscous cross flow is represented by a potential flow model in which a pair of symmetrically disposed vortices are attached to the cylindrical cross section at each axial station. The motion and the strength of the vortices, which are connected to the cylinder by a feeding sheet of vorticity, can be computed for the case of the impulsively started cylinder when the separation points on the cylinder are known. By using the impulsive flow analogy and replacing the time t with $X/V_\infty \cos\alpha'$, the positions and strengths of the vortices can be computed for each axial station along the missile body. From this information, the normal force and center of pressure can be determined. The main disadvantage of such methods is that the actual separation lines along the body must be known for each angle of attack, Mach number, and Reynolds number. At present, this information must be obtained experimentally and is more difficult to measure than it is to measure the forces and moments directly.

It was recognized at the time when the previously mentioned theories were being developed that the symmetrically disposed pair of vortices was only a special case of a more complex flowfield. It was shown experimentally[13-15] that at higher angles of attack, the symmetrical vortex pair is replaced by a steady asymmetrical flow with two or more vortex cores present. At still higher angles, this steady flow is replaced by an unsteady flow in which the vortex locations switch randomly with time. Finally, as α approaches 90°, the distinct vortices may be replaced by a turbulent wake (for $R_{ed} > 10^5$). These

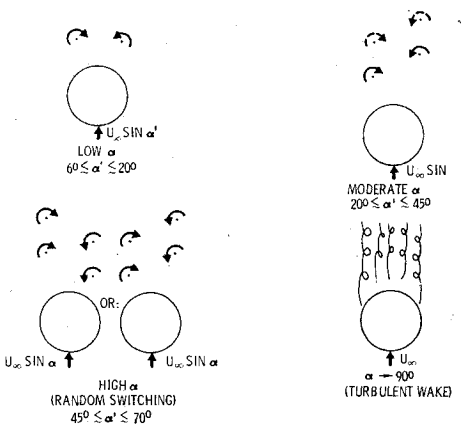

Fig. 3 Flowfield schematics illustrating viscous effects in important incidence ranges.

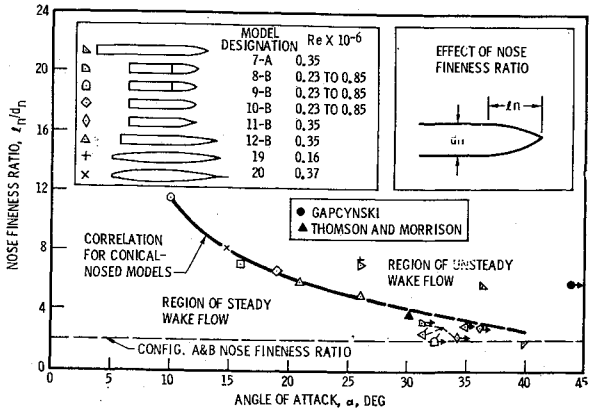

Fig. 4 Comparison of data from Gowan and Perkins[13] with that of Gapcynski and Thomson and Morrison, showing effects of nose fineness ratio on boundary between steady and unsteady wake flow.

various flowfields are characterized in Fig. 3. There is very little quantitative information describing this process. It appears that nose shape, over-all fineness ratio, cross flow Mach number, and Reynolds number all influence the angle of attack at which the various flow regimes are present. Figure 4 (which is taken from Ref. 13) illustrates the effect of nose bluntness on the incidence at which unsteady flow is observed. The unsteady flow phenomenon observed by Gowen and Perkins[13] apparently is not common to all missile configurations. For instance, Gapcynski[15] (data point as indicated on Fig. 4) did not observe any random unsteadiness in his experiments, nor did Thomson and Morrison[16] in their observations (although certain wake instabilities were noted). The present authors have observed in vapor screen tests that for the configurations to be described here, a pair of symmetrically disposed, steady vortices exist at angles of attack as high as 35° and with $M = 1.2$.

One of the few quantitative analyses dealing with asymmetrical vortices is that of Thomson and Morrison.[16] Their tests were conducted over a range of Mach numbers from $0.4 \leq M \leq 2.8$ using a cone-cylinder of high fineness ratio (greater than 25). These authors were interested in separated flows of the type shown in Fig. 5, in which the vorticity is shed alternately along the body in three-dimensional counterpart to the vortex shedding observed in the two-dimensional flow past circular cylinders. Thomson and Morrison showed that the spacing between the vortex cores can be related to the shedding frequency of circular cylinders through the equation.

Thomson and Morrison measured the spacing g' and found that the computed Strouhal number was around 0.2, which is very close to the value for a circular cylinder for subcritical Reynolds numbers. The measured value of S remained constant until the cross flow Mach number ($M_c = M \sin\alpha$) reached a value of approximately 0.7. Then S increased with increasing M_c, reaching a value of $S = 0.65$ at $M_c = 1.65$.

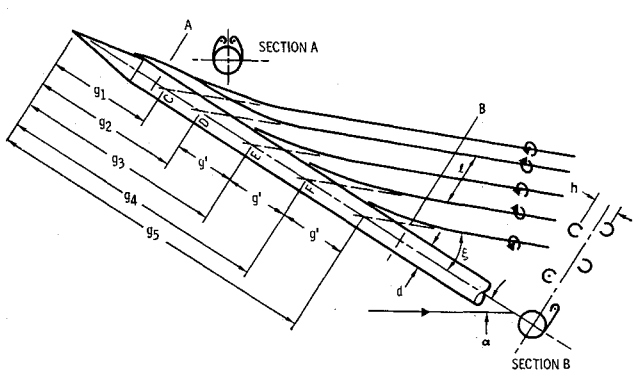

Fig. 5 Wake from slender cone-cylinder at large incidence (from Ref. 16).

These experiments were conducted at low cross flow Reynolds numbers of less than 8×10^4. Krouse[17] investigated the flow around a tangent-ogive-cylinder with nose length-to-diameter ratio of 4.89 and over-all fineness ratio of 10 for Mach numbers of 0.55 and 0.80, and cross flow Reynolds numbers in the range $4.5 \times 10^5 < R_c < 8 \times 10^5$. From Krouse's Fig. 4 (Ref. 17), the Strouhal number calculated from Eq. (4) is approximately $S = 0.3$ at $M_c = 0.4$ and $\alpha = 30°$. Pick[18] conducted similar investigations for ogive-cylinders with various nose bluntnesses and over-all fineness ratio of approximately 11 for $0.5 < M < 1.1$ and at subcritical Reynolds numbers. According to Pick, the measured Strouhal numbers for all the configurations tested were in the range $0.19 < S < 0.30$. Both Krouse and Pick used missile shapes of low fineness ratio (compared to that of Thomson and Morrison), and the observed vortex structure was probably strongly influenced by the nose shape. Hence, a strictly two-dimensional analogy does not seem sufficient to characterize the flowfield accurately, except for the case of high fineness ratio, where the nose influence is not strongly felt for downstream axial stations.

The occurrence of asymmetrical vortices is accompanied by side forces and yawing moments that can be of considerable magnitude. This asymmetrical loading must be accounted for in the design of missiles that maneuver at angles of attack at which asymmetrical flows can occur. In addition to the experiments described in this paper, several other investigators have recently studied this phenomenon. Krouse[17] measured side forces that were approximately 60% to 70% as large as the lift force on the tangent-ogive cylinder described previously. These large side forces occurred at angles of attack in the range $30° < \alpha' < 40°$. Pick[18] studied the effects of nose fineness and bluntness ratio on the magnitude of the side forces produced by asymmetrical flow separation on ogive-cylinder bodies. His general conclusion was that an increase in nose bluntness resulted in a decrease in the maximum side force. Also, an increase in nose fineness resulted in an increase in the side force for sharp noses or for noses with little bluntness. However, for noses with 20% bluntness ratio (defined as the ratio of nose radius to cylindrical afterbody radius) the side force decreased with increasing nose fineness.

Occurrence of Induced Yawing Moments during Wind-Tunnel Tests of Configurations A and B

Wind-tunnel testing of configurations A and B (illustrated in Fig. 6) was conducted largely at the McDonnell Douglas Aerophysics Lab. (MDAL) Four-Foot Trisonic Wind Tunnel (4TWT) in El Segundo, Calif., with some supplementary testing in the Naval Ship R&D Center (NSRDC) 7- by 10-ft wind tunnel. The MDAL 4TWT is a blowdown-to-atmosphere facility that can operate at velocities from a few tens-of-feet-per-second to Mach 5.0. One of the prime distinctions of this wind tunnel is its high unit Reynolds number

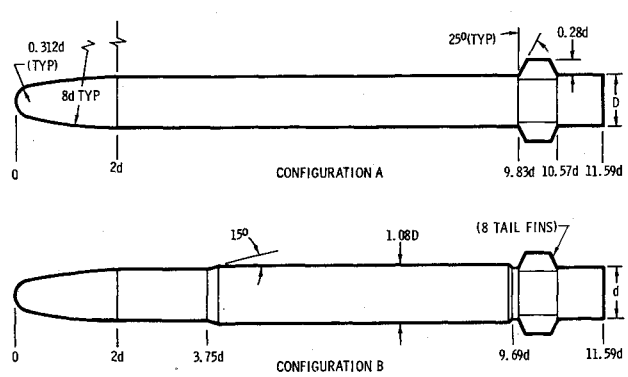

Fig. 6 Configurations tested.

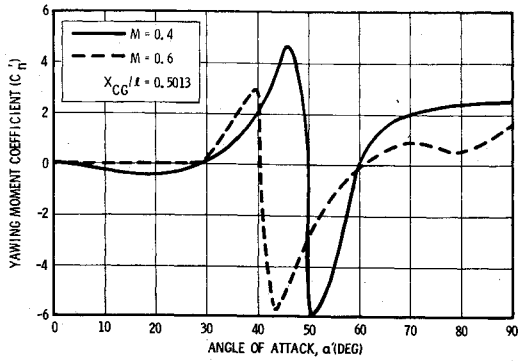

Fig. 7 C_n' data for configuration A.

capability. Detailed operating characteristics of the 4TWT may be found in Ref. 19.

Yawing moments (acting perpendicular to the relative pitch plane) were first observed during testing of configuration A, when substantial yawing moment coefficients (C_n') were observed at $M = 0.4$ and 0.6 (Fig. 7). The literature dealing with viscous effects at high incidence indicated that the observed yawing moments were probably induced by asymmetries in the model wake. Figure 8 shows a comparison of some data from Fig. 7 with C_n' data measured with the same model and balance system in the NSRDC 7- by 10-ft wind tunnel with tail on and off at $M = 0.6$. All the data compare favorably. Thus, it would appear that the model tail fins play a very small role in the root causes of the induced yawing moments.

To establish the contribution (if any) of Magnus effects to the yawing moment, a wind-tunnel test of configurations A and B was conducted with the models driven in roll from 0 to 10 rps. Angles of attack from 5° to 45° and Mach numbers from 0.4 to 1.2 were investigated. Side forces and yawing moments observed in this test harmonically oscillated plus-to-minus. The largest yawing moment amplitude (worst case) occurred at $\alpha' = 35°$ and $M = 0.8$. Figure 9 shows the time history of this condition where α' and M were constant and the model spin frequency decayed from 10 rps to 0 rps. Harmonic analysis of the data, after deletion of inertial effects, is shown in Fig. 10, which indicates that the fundamental amplitude was essentially independent of frequency. The fact that the yawing moment switches sign with model roll position and is independent of frequency leads to the conclusion that it is not caused by Magnus effects.

Gowen and Perkins[13] traced the occurence of asymmetric disposition of wake vortices at a given α' to the presence of minute rotational asymmetries in the model nose (adjunct to standard fabrication tolerances). For our current testing,

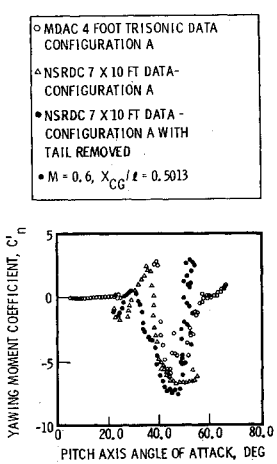

Fig. 8 Comparison of C_n' data from MDAL and NSRDC using the same model and balance.

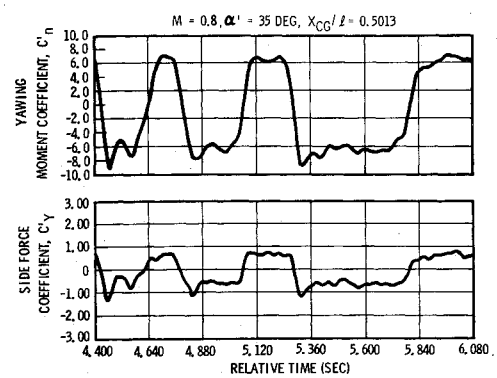

Fig. 9 Lateral data for configuration B.

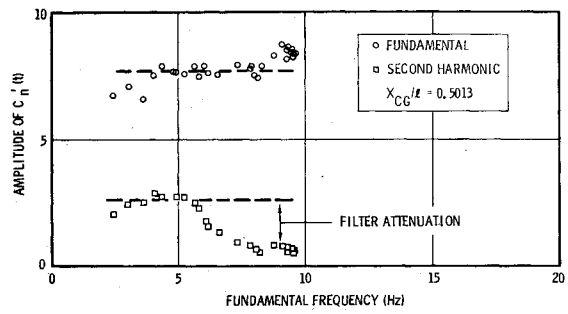

Fig. 10 $C_n'(t)$ amplitudes from harmonic analysis.

the model body dimensions (cylindrical) were precise to within ±0.002 in.; however, the model nose runout was found to be ±0.004 in. near its tip, as illustrated in Fig. 11. The nature of the nose asymmetries may be interpreted as a 0.051° misalignment of the nose centerline relative to the model centerline.

A subsequent wind-tunnel test was conducted at conditions of the most concern (i.e., $M = 0.8$ and $25° < \alpha' < 45°$) to study the effects of various discrete nose and body bank angles and various configurational perturbations upon occurrence of the induced yawing moments.

Small changes in model nose and body bank angle were independently observed to induce large changes in the C_n'

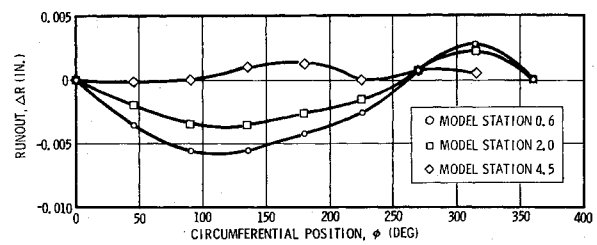

Fig. 11 Some runout characteristics of the N_6 nose.

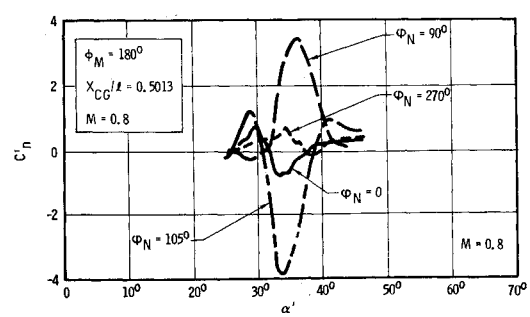

Fig. 12 Nose bank angle effects with model body bank angle fixed (configuration A).

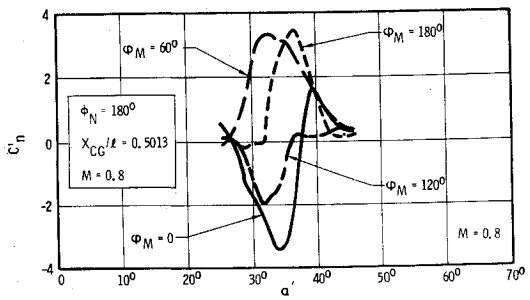

Fig. 13 Body bank angle effects, nose bank angle fixed (configuration A).

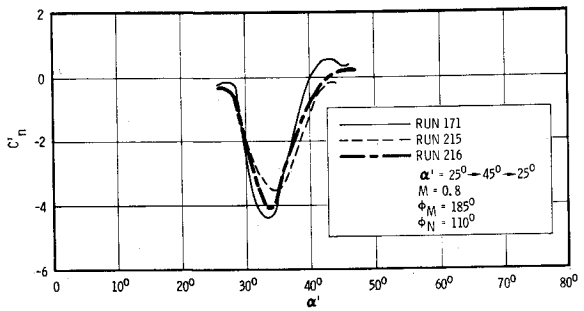

Fig. 14 Repeatability of yawing moment data (configuration A).

characteristics, as illustrated in Figs. 12 and 13. The nose and model body bank positions are measured clockwise looking forward. The leeward generator corresponds to $\phi = 0$. The marked sensitivity of C_n' to nose and body bank angle was probably a result of the wake vortices changing positions as a function of the different minute asymmetries operating on the flow at each bank condition. It is of interest to notice that the flow is as sensitive to body bank orientation as it is to nose bank orientation.

Figure 14 illustrates the repeatability of the C_n' data at a nose-and-body bank-angle combination that seemed to produce maximum values of C_n'. When the configuration was "complicated" with a slight ramp to a slightly increased body diameter at about $X/d = 4$ (configuration B), the C_n' data were not repeatable. A lack of precise data repeatability is indicative of a possibly unsteady flowfield.

Various arrangements of carborundum grit bonded to the nose were tested to evaluate their performance in regularizing boundary-layer turbulence and (resultingly) wake stability. In addition, two versions of "vortex generator collars" consisting of 36 small winglets mounted in the region of initial vortex separation (on the nose) were tested (Fig. 15). This sort of

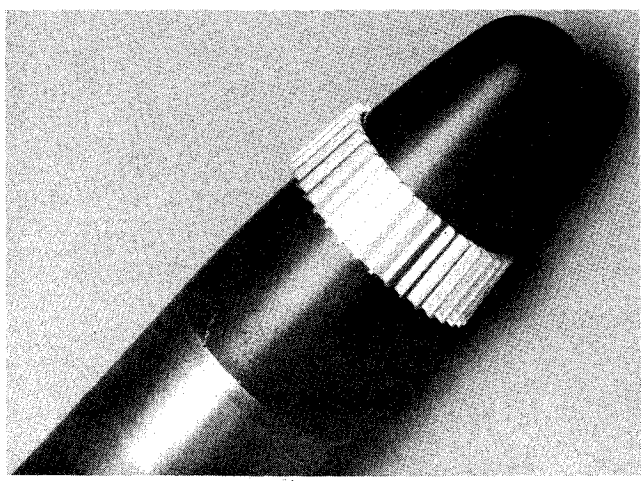

Fig. 15 Nose-mounted vortex generator.

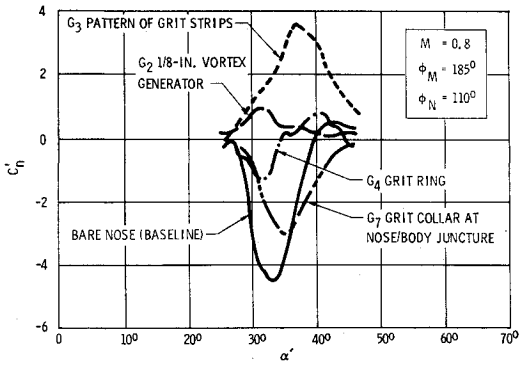

Fig. 16 Effects of nose-mounted flowfield disturbance techniques, configuration A.

device is hypothesized to produce a regularized, symmetric field of discrete vortices that may alter the fundamental processes that lead to separation of the cross flow boundary layer and subsequent rollup of free vortex layers into regions of concentrated vorticity. The end result sought is alteration of the wake flowfield to the extent that either asymmetric strong vortices will then not form close to the missile body, or the vortices will be inhibited from becoming asymmetrically disposed.

The influence of the various flowfield disturbance devices previously noted upon the character of the yawing moments is illustrated in Fig. 16. Of the methods tested, the vortex generator device proved the most successful in systematically reducing the maximum observed values of C_n', as evidenced by comparison of Fig. 17a with Fig. 17b. Figure 17a illustrates the locus of maximum C_n' values from a montage of 12 runs at 12 differing bank angles for configuration B without

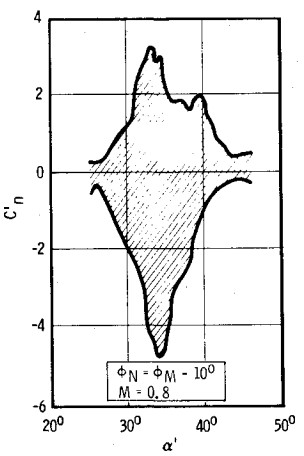

a) WITHOUT VORTEX GENERATOR

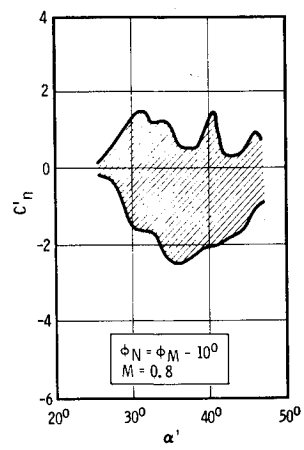

b) WITH VORTEX GENERATOR

Fig. 17 Yawing moment coefficient locus of maximum values from 12 runs at $\phi_M = 0$ to 330° in 30° increments (configuration B).

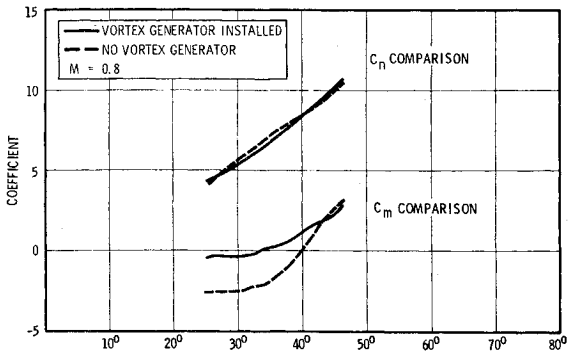

Fig. 18 Effects of vortex generator on normal force and pitching moment.

the vortex generator installed. Figure 17b illustrates another locus of maximum C_n' values measured using the same 12 bank positions and model, but with the vortex generator collar installed. As may be noted in the comparison, the vortex generator method was successful in producing a factor-of-2 reduction in the maximum observed value of C_n'. Figure 18 illustrates the effect of the vortex generator device upon normal force and pitching moment coefficients for configuration A.

Flow Visualization Experiments

A series of tests was conducted using configuration A (Fig. 6) without the tail fin assembly to characterize the basic flowfield. The primary objective was to make visual observations of the flows and to establish the mechanisms concerning why the addition of flowfield disturbance devices is effective in reducing yawing moments. In these tests, schlieren photography, surface oil-flow, and vapor screen observations were used to study the body flowfields. Figures 19 and 20 show typical schlieren photographs from a series of angles of attack of Mach = 0.8 with Reynolds number of 2.03×10^6 (based on body diameter). There was no observable indication of asymmetric wake vortices or alternate shedding of vortices until an angle of attack of 50° was reached, although certain asymmetries were observable at $\alpha = 32°$ in the oil-flow patterns. Figure 20 shows a schlieren photograph taken during a run for which there are no corresponding oil-flow data. The wake vortices are apparently asymmetrically disposed at this condition ($M = 0.8$, $\alpha \approx 32°$, $R_{ed} = 2.03 \times 10^6$) over the model aft portions, resulting in a yawing moment coefficient of about −2.48.

The separation lines measured from surface oil-flow studies for $\alpha' = 15°$, 32°, 52°, and 72° ($M = 0.8$, $R_{ed} = 2.03 \times 10^6$) are illustrated in Fig. 21. Figures 22–25 show photographs

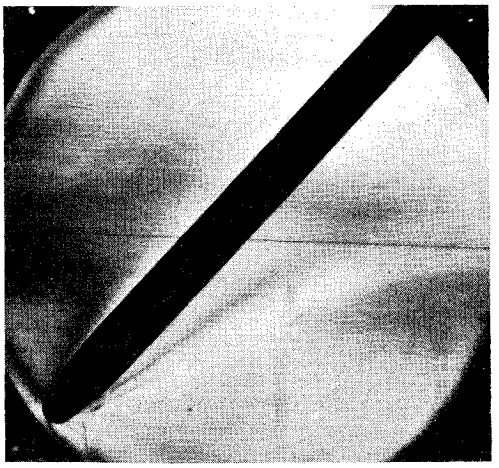

Fig. 19 Schlieren photo, $M = 0.8$, $\alpha' = 50°$, $R_{ed} = 2.03 \times 10^6$.

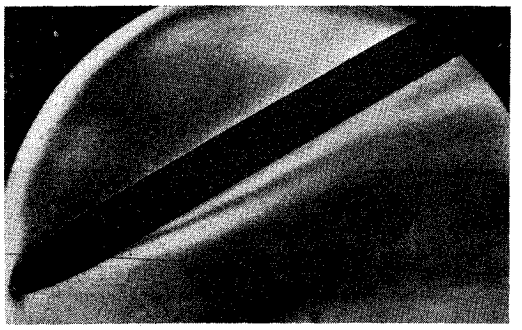

Fig. 20 Schlieren photo, $M = 0.8$, $\alpha' = 32°$, $R_{ed} = 2.03 \times 10^6$.

of typical oil-flow patterns from which these measurements were made. Figure 26 shows schlieren photos taken at Mach = 0.4 for three angles of attack ($\alpha' = 36°$, 48°, and 53°). Reynolds number was held approximately constant for the Mach = 0.4 ($R_{ed} = 1.8 \times 10^6$) and Mach = 0.8 ($R_{ed} = 2.03 \times 10^6$) flows. In the $M = 0.4$ case, there is a clear breakaway of the vortices, resulting in a picture similar to that illustrated in Fig. 5. Unfortunately, the separate vortex cores are not shown with sufficient distinction to compute the Strouhal number from Eq. (4).

From the measured separation lines shown in Fig. 21, the vortex positions and strengths and the normal force and pitching moment coefficients were computed by the method presented in Ref. 12. These theoretical values are compared

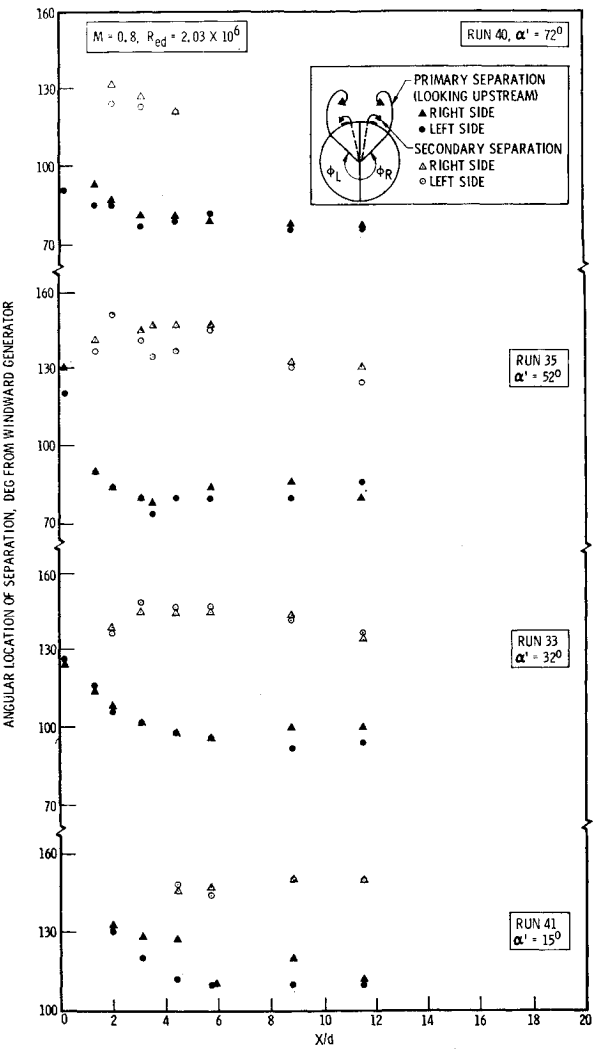

Fig. 21 Separation lines as measured from surface oil-flow experiments.

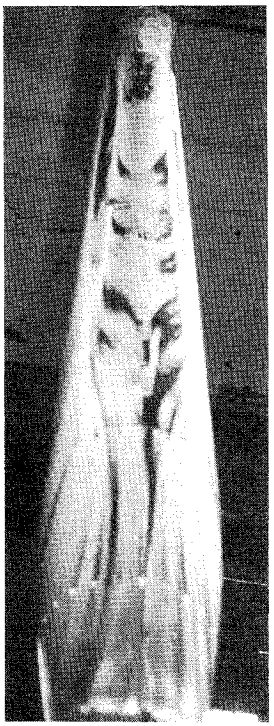

Fig. 22 Surface oil-flow pattern, $M = 0.8$, $\alpha' = 15°$, $R_{ed} = 2.03 \times 10^6$ (view of lee side from nose).

in Figs. 27 and 28 with the measured normal force and pitching moment coefficients.

Figure 29 shows a schlieren photograph taken of the flowfield about configuration A (without tail assembly) with a substantial flowfield disturbance device of the vortex generator type installed ($M = 0.8$, $R_{ed} = 2.03 \times 10^6$, $\alpha' = 32°$). Figure 30 shows corresponding separation lines as derived from oil-flow measurements. Comparison of Figs. 27 and 30 with Figs. 20 and 21 reveals that the vortex generator had a profound effect upon the wake flowfield, the quantitative effects of which are not currently understood. Figure 31 shows photographs of the oil-flow pattern resulting from the vortex generator device. At $M = 0.8$, $\alpha' = 32°$, and $R_{ed} = 2.03 \times 10^6$, addition of the vortex generator device to configuration

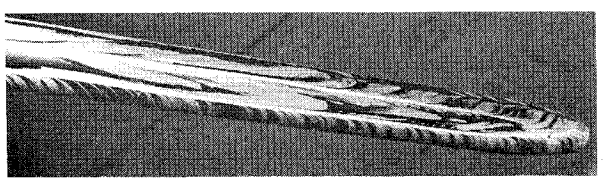

Fig. 23 Surface oil-flow pattern, $M = 0.8$, $\alpha' = 32°$, $R_{ed} = 2.03 \times 10^6$ (side view).

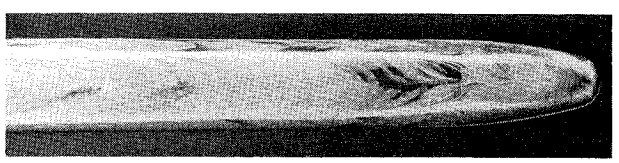

Fig. 24 Surface oil-flow pattern, $M = 0.8$, $\alpha' = 52°$, $R_{ed} = 2.03 \times 10^6$ (view looking down at leeward generator).

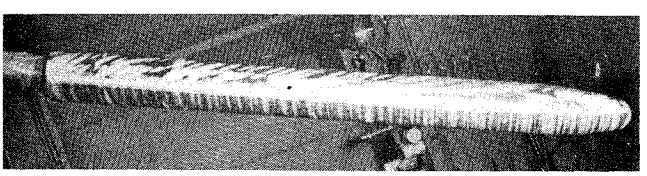

Fig. 25 Surface oil-flow pattern, $M = 0.8$, $\alpha' = 72°$, $R_{ed} = 2.03 \times 10^6$ (side view).

a) α' = 36 DEG

b) α' = 48 DEG

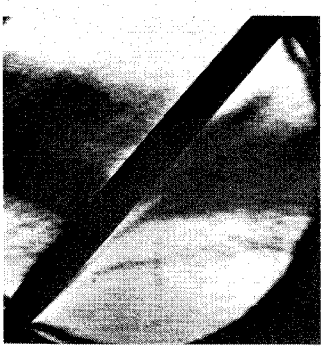

c) α' = 53 DEG

Fig. 26 Schlieren photos, $M = 0.4$, $R_{ed} = 1.8 \times 10^6$.

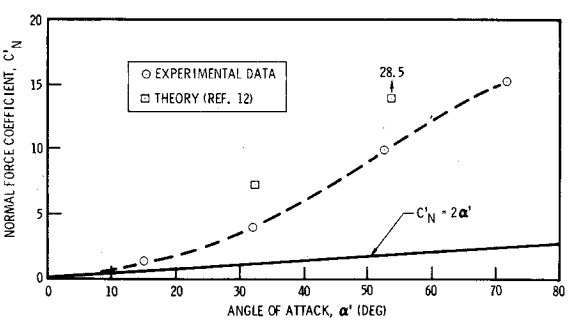

Fig. 27 Normal force coefficients.

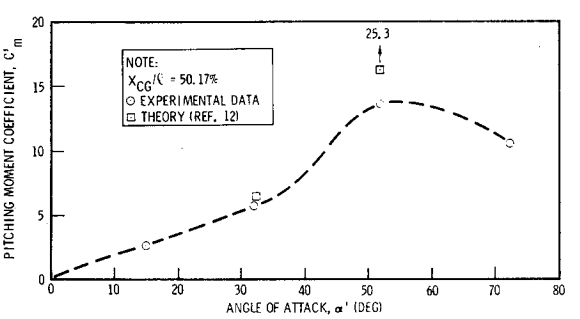

Fig. 28 Pitching moment coefficients.

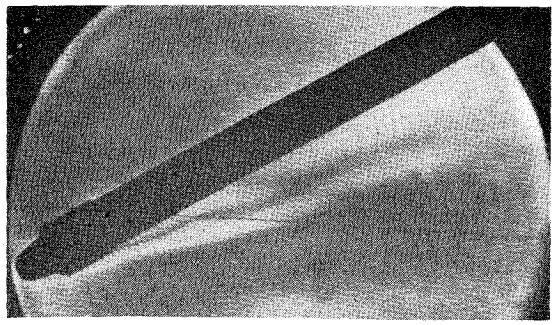

Fig. 29 Schlieren photo, $M = 0.8$, $\alpha' = 32°$, $R_{ed} = 2.03 \times 10^6$, vortex generator installed.

A with tail fins off was successful in reducing the observed yawing moment coefficient from −2.48 to −1.01.

Dealing with the Yawing Moments: Root Causes and Possible Remedial Measures

Experimental information[13-15] establishes the existence of conditions wherein asymmetrically disposed, steady vortices may be formed in body-of-revolution wakes at high incidence. References 17 and 18 (as well as many other sources not cited) and this paper established a strong correlation between asymmetrically disposed wake vortices and occurrence of large side forces and yawing moments.

To study analytically the sort of wake vortex asymmetries that may induce large side forces and yawing moments, the method of Ref. 20 was automated and employed to calculate vortex pair trajectories and resulting side force and yawing moment coefficients induced upon a circular cylinder at 25° angle of attack. In Ref. 20, the vortices are assumed to be of constant strength along the body axis. This assumption is

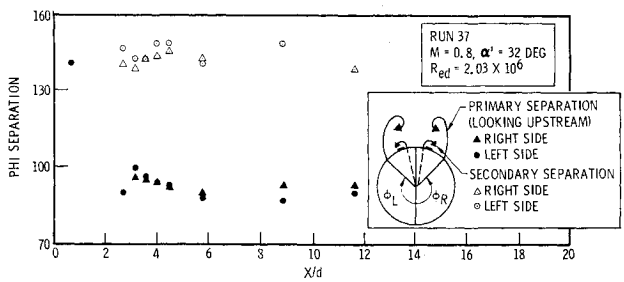

Fig. 30 Separation lines as measured from surface oil-flow experiments, vortex generator nose.

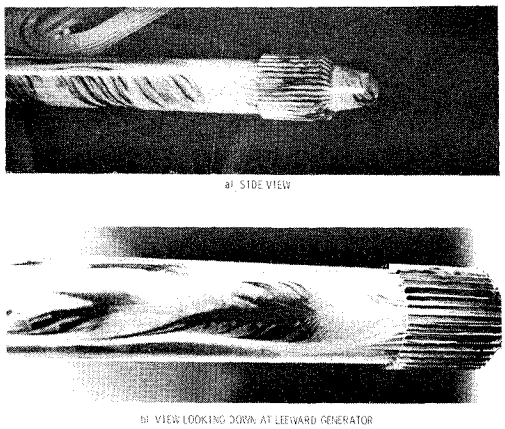

Fig. 31 Surface oil-flow pattern, vortex generator nose, $M = 0.8$, $\alpha' = 32°$, $R_{ed} = 2.03 \times 10^6$.

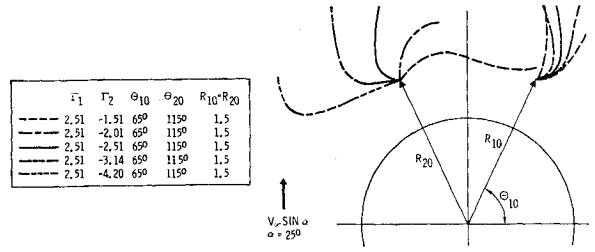

Fig. 32 Vortex trajectories showing effects of varying Γ_2.

not realistic for the present case, in which there is a continual increase in vortex strength due to accumulation of vorticity from the cross flow boundary layer. Nevertheless, the effects of flowfield asymmetries can be conveniently explored in a qualitative sense using the techniques of Ref. 20. Three methods of introducing asymmetries in the flowfields were explored. 1) Vortices symmetrically disposed at Station 0, but having unequal circulation (strength) (Figs. 32–34). 2) Vortices having equal strength and initial radius from the cylinder centerline, but with different initial polar angles (with respect to right-hand horizontal ray) (Figs. 35–37). 3) Vortices having equal strength and initial polar angle, but positioned at differing initial radii (Figs. 38–40).

Study of Figs. 32–40 shows that asymmetries in vortex strength and initial radial position induce the largest side forces and yawing moments, as well as the most asymmetrical vortex trajectories.

The vortex trajectories that result from asymmetries in vortex strength (Fig. 32) exhibit somewhat irrational behavior in terms of what has been observed experimentally. Therefore, dispositiion of equal-strength vortices at differing radii from the missile centerline appears to best represent the initial

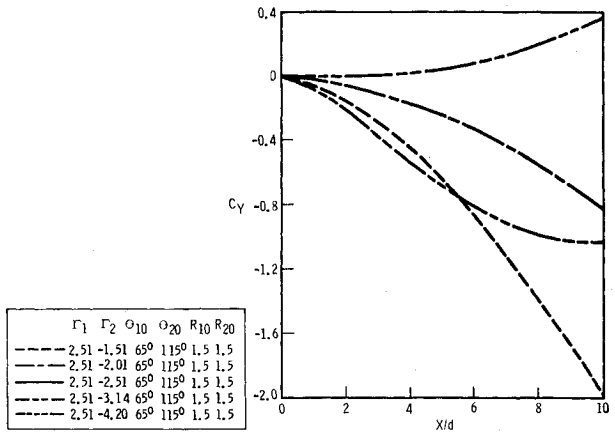

Fig. 33 C_Y vs X/d for varying Γ_2, $\alpha = 25°$.

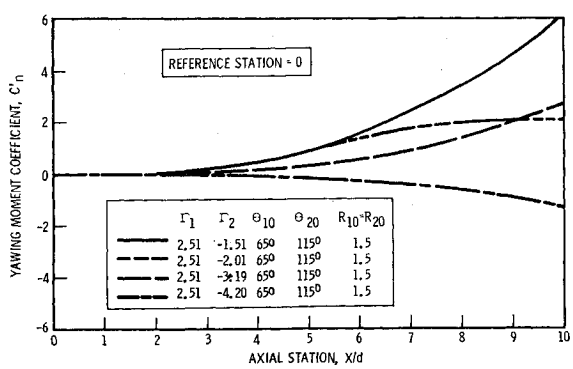

Fig. 34 Yawing moment coefficients induced by varying Γ_2.

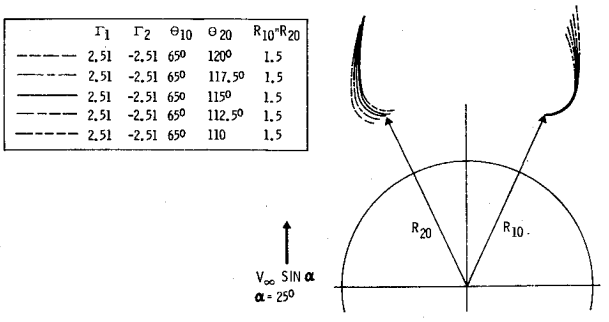

Fig. 35 Vortex trajectories showing effects of varying θ_{20}.

conditions and resulting trajectories associated with occurrence of side forces and yawing moments induced by asymmetrical vortex wakes.

Apparently, symmetric disposition of identical or nearly identical vortices represents an unstable condition throughout a significant range of angle of attack, with the degree of instability increasing as the incidence where alternate shedding occurs is approached. When this unstable condition leads to asymmetric disposition of the wake vortices, a new condition of stability is achieved for the given incidence angle, Mach number, and Reynolds number. The resultant increasingly asymmetrical disposition of the wake vortices with increasing incidence angle eventually leads to shedding of free vortices in the wake in the familiar alternate shedding, or "vortex street" configuration.

Occurrence of asymmetrical vortices in the wakes of missiles flying at high incidence, and the resulting yawing moment disturbances, may be dealt with in either of the following ways: 1) brute force: provide sufficient control authority and autopilot gain margin to maintain flight control; or 2) dominate the wake development with a symmetrical disturbance (or disturbances) so that the wake vortices are a) forced to follow more symmetrical trajectories, b) subjected to unsteady alternate shedding induced at lower angles of attack, thus eliminating the formation of steady, asymmetrical vortices, or c) displaced away from the missile body, this reducing their effects on body airloads (with resultant loss of lift). The vortex generator devices just described apparently provide sufficient disturbance to the wake flowfield to cause the wake vortices to be more symmetrically disposed in the critical incidence and Mach number region ($M \approx 0.8$, $30° \geq \alpha' \geq 40°$). The mechanics of this result are not quantitatively understood at this juncture.

Conclusions

It is concluded that significant yawing moments and side forces may be induced by stable, asymmetrical disposition of vortices in the wakes of blunt bodies of revolution flying at high incidence with cross flow Mach numbers in the subsonic

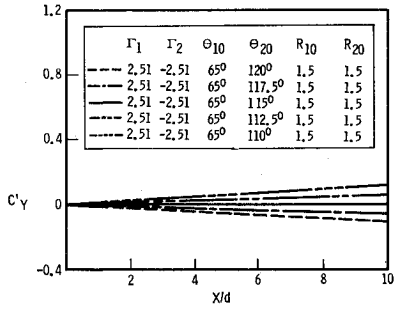

Fig. 36 C_Y' vs X/d for varying θ_{20}, $\alpha = 25°$.

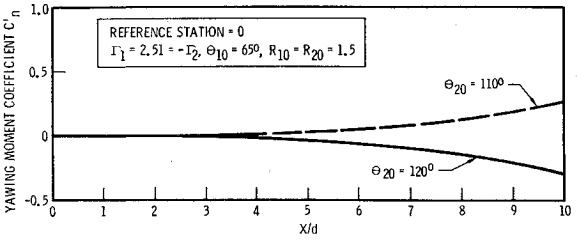

Fig. 37 Yawing moment coefficient induced by varying θ_{20}.

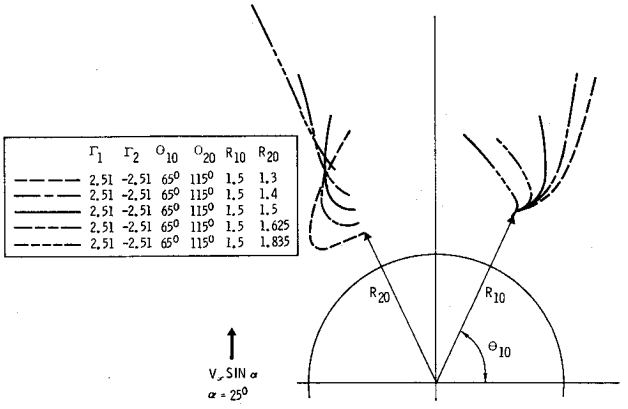

Fig. 38 Vortex trajectories showing effects of varying R_{20}.

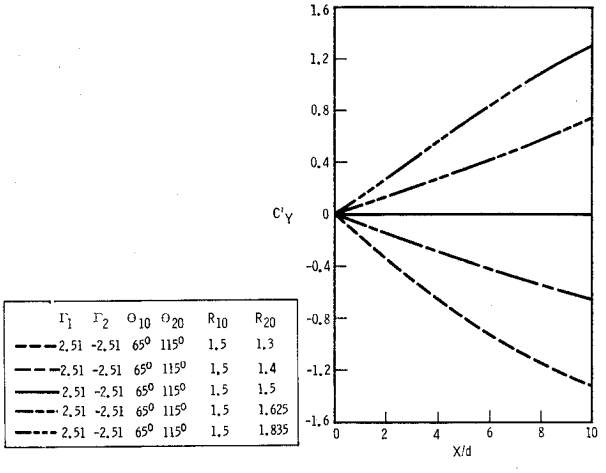

Fig. 39 C_Y' vs X/d for varying R_{20}, $\alpha = 25°$.

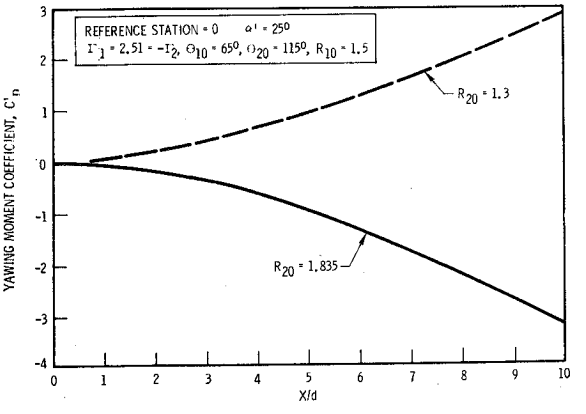

Fig. 40 Yawing moment coefficients induced by varying R_{20}.

range and with cross flow Reynolds numbers well above critical values. Such induced yawing moments and side forces may be substantially reduced by addition of certain flowfield disturbance devices that significantly alter the wake development processes.

Discrepancies between the flowfield observations reported here and those of authors whose experiments were performed at critical and subcritical Reynolds numbers underscore the importance of simulating Reynolds numbers that duplicate critical flight conditions of the particular missile airframe under consideration.

Although certain missile and rocket systems have been developed that fly at angles of attack high enough to encounter large induced yawing moments, very little quantitative information is available concerning the root causes and effects of asymmetrical vortex wakes in Mach number and Reynolds number regimes of practical interest. Less information is available concerning the alteration of such phenomena for purposes of maintaining flight control. The authors of this paper feel that much remains to be learned about viscous effects at high incidence before flight of highly maneuverable missiles at such conditions becomes an everyday matter. The current state of the art remains more speculative than quantitative because new experiments always seem to pose more questions than answers.

References

[1] Munk M. M., "The Aerodynamic Forces on Airship Hulls," Rept. 184, 1924, NACA.

[2] Allen, H. H. and Perkins, E. W., "A Study of Effects of Viscosity on Flow Over Slender Inclined Bodies of Revolution," TR 1048, 1951, NACA.

[3] Tsien, H. S., "Supersonic Flow Over an Inclined Body of Revolution," *Journal of the Aeronautical Sciences*, Vol. 5, No. 12, Oct. 1938, pp. 480–483.

[4] Van Dyke, M. D., "First and Second Order Theory of Supersonic Flow Past Bodies of Revolution," *Journal of the Aeronautical Sciences*, Vol. 18, No. 3, March 1951, pp. 161–178.

[5] Perkins, E. W. and Jorgenson, L. H., "Comparison of Experimental and Theoretical Normal Force Distributions (Including Reynolds Number Effects) of an Ogive Cylinder Body at Mach No. 1.98," TN 3716, 1956, NACA.

[6] Milne-Thomson, L. M., *Theoretical Hydrodynamics*, MacMillan, New York, 1960, Plate 1.

[7] Kelly, H. R., "The Estimation of Normal Force, Drag, and Pitching Moment Coefficients for Blunt Based Bodies of Revolution at Large Angles of Attack," *Journal of the Aeronautical Sciences*, Vol. 21, No. 8, Aug. 1954, pp. 549–555.

[8] Schwabe, M., "Pressure Distribution in Nonuniform Two-Dimensional Flow," TM 1039, 1943, NACA.

[9] Sarpkaya, T., "Separated Flow About Lifting Bodies and Impulsive Flow About Cylinders," *AIAA Journal*, Vol. 4, No. 3, March 1966, pp. 414–420.

[10] Bryson, A. E., "Symmetric Vortex Separation on Circular Cylinders and Cones," *Journal of Applied Mechanics*, Vol. 26, No. 4, Dec. 1959, pp. 643–648.

[11] Schindel, L. H., "Effect of Vortex Separation on the Lift Distribution on Bodies of Elliptic Cross Section," *Journal of Aircraft*, Vol. 6, No. 6, June 1969, pp. 537–543.

[12] Angelucci, S. B., "A Multivortex Method for Axisymmetric Bodies at Angles of Attack," *Journal of Aircraft*, Vol. 8, No. 12, Dec. 1971, pp. 959–966.

[13] Gowen, F. E. and Perkins, E. W., "Study of the Effects of Body Shape on the Vortex Wakes of Inclined Bodies at $M = 2$," RM A53117, 1953, NACA.

[14] Mead, M. H., "Observations of Unsteady Flow Phenomena for an Inclined Body Fitted with Stabilizing Fins," RM A51K05, Jan. 1952, NACA.

[15] Gapcynski, J. P., "An Experimental Investigation of the Flow Phenomena Over Bodies at High Angles of Attack at a Mach Number of 2.01," RM L55H29, Oct. 1955, NACA.

[16] Thomson, K. D. and Morrison, D. F., "The Spacing, Position, and Strength of Vortices in the Wake of Slender Cylindrical Bodies at Large Incidence," *Journal of Fluid Mechanics*, Vol. 50, Pt. 4, 1971, pp. 751–783.

[17] Krouse, J. R., "Induced Side Forces on Slender Bodies at High Angles of Attack and Mach Numbers of 0.55 and 0.8," AL-79, May 1971, Naval Ship R & D Center, Washington, D.C.

[18] Pick, G. S., "Investigation of Side Forces on Ogive Cylinder Bodies at High Angles of Attack in the $M = 0.5$ to 1.1 Range," *Journal of Spacecraft and Rockets*, Vol. 9, No. 6, June 1972, pp. 389–390.

[19] Raddatz, L. A., "The Douglas Aerophysics Laboratory Four-Foot Trisonic Wind Tunnel," Rept. DAC-5909, Oct. 1967, Douglas Aircraft Co., Santa Monica, Calif.

[20] Spahr, J. R., "Theoretical Prediction of the Effects of Vortex Flows on the Loading, Forces, and Moments of Slender Aircraft," TR R101, 1961, NASA.